Navarro-Cavallé, J., Wijnen, M., Fajardo, P. & Ahedo, E. (2018). Experimental characterization of a 1 kW Helicon Plasma Thruster. *Vacuum*, vol. 149, pp. 69–73.

DOI: 10.1016/j.vacuum.2017.11.036

Experimental characterization of a 1 kW Helicon Plasma Thruster

Navarro-Cavallé, J., Wijnen, M., Fajardo, P., and Ahedo, E.

Equipo de Propulsión Espacial y Plasmas, Universidad Carlos III de Madrid

Avenida de la Universidad 30, 28911 Leganés, Spain

Abstract

A Helicon Plasma Thruster has been tested in the 500 - 1000 W radio-frequency power range, at 13.56 MHz. In order to determine its propulsive performances, a parametric study of some operational parameters has been carried out, including the exploration of the magnetic field topology and strength, the mass flow rate, and different propellants. The plasma plume has been characterized by means of intrusive plasma diagnostics, which allow an indirect estimation of the thrust, 2 - 6.6 mN, and thrust efficiency, about 2.9 %. The structure of the plasma expansion is compared against a theoretical model showing a good agreement.

Keywords: `space propulsion, helicon plasma thruster, experimental plasmas`

The Helicon Plasma Thruster (HPT) [1, 2, 3] has been proposed recently as a reliable technology for in-Space Electric Propulsion. This concept is essentially based on the use of a Helicon Source [4, 5] to produce a dense plasma and accelerate it supersonically in a second stage, called Magnetic Nozzle (MN), which is mainly a divergent magnetic field. The neutral gas is ionized and heated by radio-frequency (RF) radiation in the MHz range. Some advantages against other mature devices, such as the Ion Gridded or the Hall Effect Thrusters [6], have been underlined by the Electric Propulsion community [7, 8, 9]: the lack of electrodes, the flexibility in the propellant choice and throttleability (variable thrust and specific impulse) by tuning its operational parameters, a long lifetime

(thanks to the magnetic screening of its walls), and even thrust vectoring [10].

This work inquires into the evaluation of the propulsive performances of the HPT05 breadboard, a prototype that has been conceived by the EP2-UC3M[1] based on their theoretical background of the plasma phenomena [11, 12, 13], and manufactured by SENER[2]. The HTP05 design is a downgraded escalation in power of the results compiled in an European Space Agency funded project [14] carried out by the aforementioned institutions.

The HPT05 consists of a classical HPT architecture composed of the following elements (see Figure 1): a cylindrical chamber, where the plasma is produced; a magnetic circuit to generate the magnetic field, which allows coupling RF power more efficiently to the plasma, confining the plasma, and guiding and expanding it on the MN; a RF system to emit the RF wave; and an injector system to feed the thruster with the neutral gas, Argon or Xenon in our case.

The discharge chamber is made of quartz, 30 mm inner diameter, and variable length, 150 - 280 mm. The length is modified by sliding the ceramic injector piston along the tube. The magnetic circuit is composed of an arrangement of three electromagnets: two of them (S1, S2) generate the quasiaxial magnetic field within the tube and the other one (S3) generates the divergent field (MN shape), being the magnetic throat (i.e. maximum magnetic field) located close to the exit section. The strength of the magnetic field can be adjusted up to 800 G. The topology of the field can be modified by inverting the polarity of the electromagnets, thus introducing magnetic separatrices and cusps. The RF wave is radiated by a double loop antenna wrapped on the quartz tube and allocated between two of the electromagnets. The antenna is fed with RF power at 13.56 MHz. Power is generated with a 2 kW amplifier and conditioned to the antenna impedance by using a π - configuration matching network. The antenna is connected to the matching circuit using a rigid transmission line

[1] EP2: Plasmas and Space Propulsion Team, research group affiliated to the Universidad Carlos III de Madrid (UC3M).

[2] SENER Ingeniería y Sistemas: it is a Spanish Engineering Company.

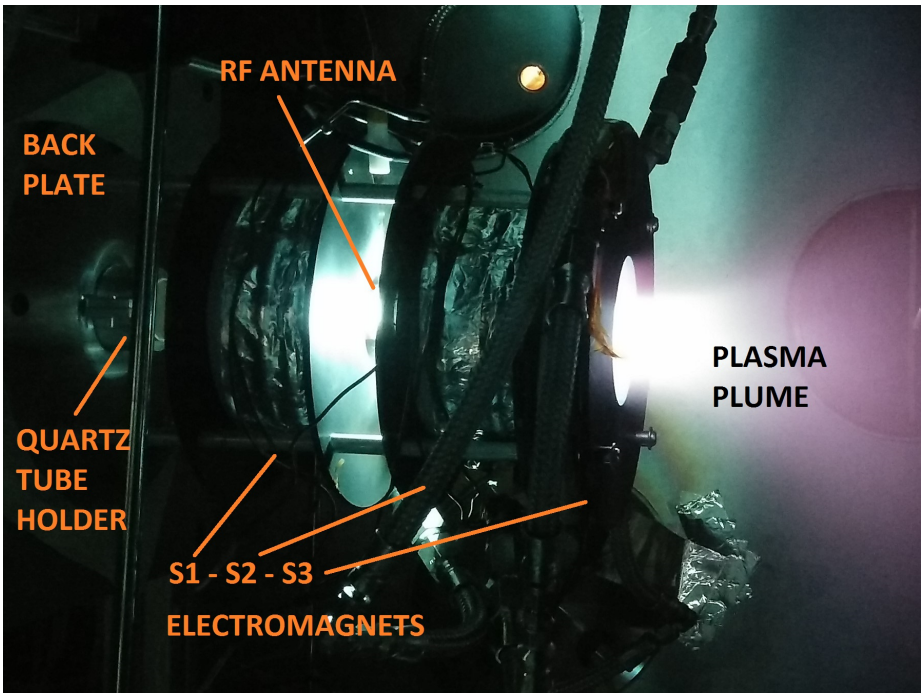

Figure 1: HPT05 firing with Xenon in the UC3M vacuum chamber. The main components are labelled in the figure.

(short in comparison to RF wavelength). During all the tests performed, forward and reflected powers have been monitored, and the second one minimized by tuning properly the variable vacuum capacitors of the mentioned matching network. Hereafter, the term RF power refers to the delivered power (difference between forward and backward) at the RF load, that is antenna and plasma column. We implicitly assume that power dissipated at the matching circuit is negligible. However, this does not imply that all delivered power is effectively coupled to the plasma; for example, part of it is lost due to thermal heating of the transmission lines and the antenna itself.

The thruster breadboard has been tested within a new vacuum chamber designed specifically to characterize Electric Propulsion Plasma Thrusters up to 1.5 kW, and located at the UC3M facilities (see Figure 2). The chamber consists of a stainless-steel 304 vessel of 1.5 m inner diameter and 3.5 m long.

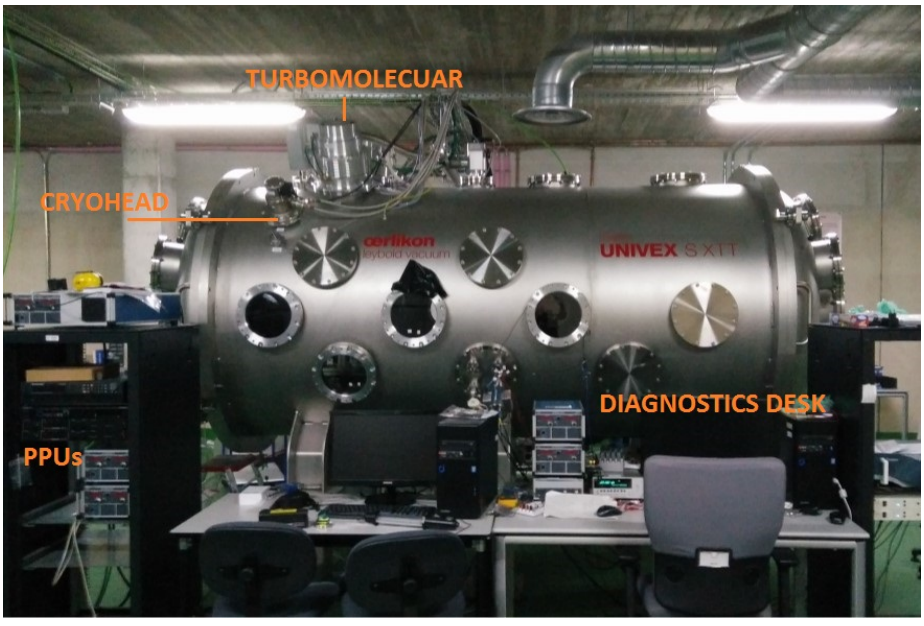

Figure 2: Photograph of the UC3M vacuum chamber for testing Electric Propulsion Plasma Thrusters.

This is equipped with three different vacuum technologies: a dry mechanical pump Leyvac LV80 with pumping speed about 80 m^3/h, a pair of turbomelecuar pumps, Leybold MAGW2.200iP with 2000 l/s of pumping speed each, and three cryopanels, Leyvac 140 T-V. The total pumping speed is about 37,000 l/s Xe, reaching an ultimate pressure of 10^{-7} mbar in dry conditions. The operational pressure is roughly $2 \cdot 10^{-5}$ mbar, when mass flow rates about 20 sccm of either Ar or Xe are injected. These are the gases typically used for Electric Propulsion plasma thrusters.

The main diagnostics employed consists of an arrangement of three different plasma intrusive probes. These have been hold on a movable arm system with three degrees-of-freedom in a Cartesian frame. The frame origin coincides with the centre of the HPT05 exit section. Coordinate z is the axial distance (on-axis) downstream of the thruster, while $x - y$ define a parallel plane to the HPT05 exit section, i.e. perpendicular to the axis line. In Figure 3, the sketch

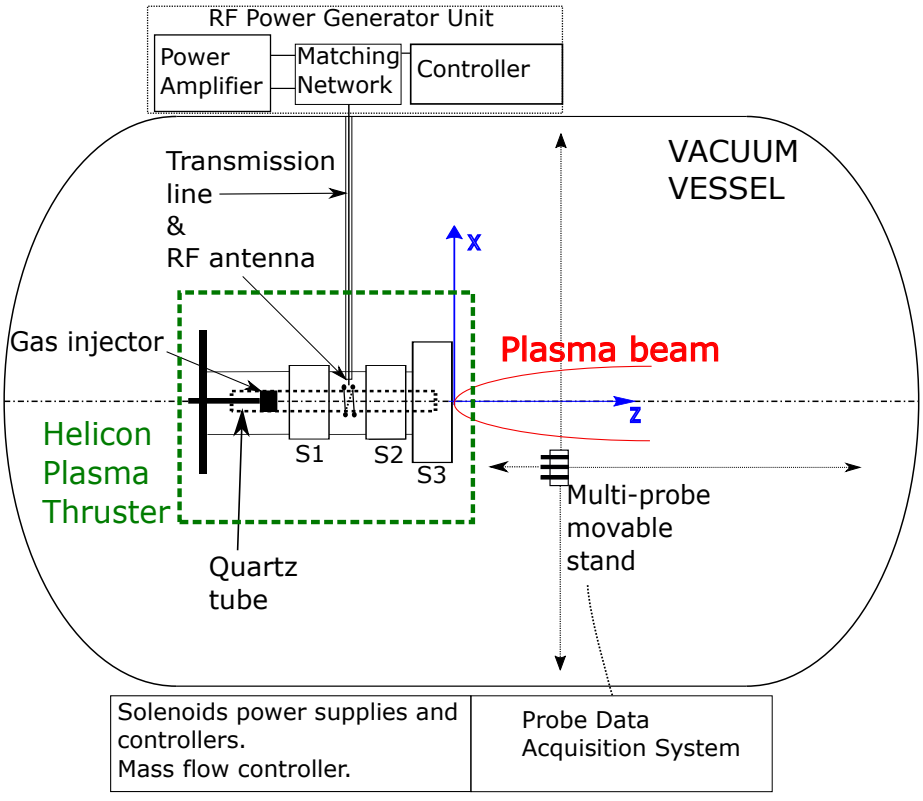

Figure 3: Sketch (not in scale) of the whole experimental setup. $x - z$ is the frame centred at the thruster exit section. S1, S2 and S3 are the solenoids to generate the magnetic field.

of the whole experimental setup is drawn, including the vacuum chamber, the HPT05 breadboard, auxiliary equipment, and diagnostics.

The mentioned probe system allows measuring time averaged spatially resolved plasma properties on the plasma beam (MN region). A single Langmuir probe (LP) is devoted to measure the plasma density n, the electron temperature T_e and the plasma potential ϕ, the last one being compared with emissive probe (EP) direct measurements. The EP is also installed on the arm system. A Faraday probe (FP) determines the ion current density j_i. The FP collector measures 10 mm in diameter, and the guard ring 11 mm ID and 20 mm OD, resulting a collector effective area of 95.03 mm^2. Concerning the LP geometry, its tip is 0.127 mm in diameter and 2 mm length and it is made of tungsten.

LP data has been postprocessed according to different classical theories: the Bernstein-Rabinowitz-Laframboise model [15], the Allen-Boyd-Reynolds model (ABR) [16], and the Bohm model (B) or planar approximation [17]. Considering the plasma properties in the HPT05 plume, there is not a clear reason to select any of the mentioned theories as the best choice. Consequently, the average between the results of the different theories is taken as a reasonable approach.

The densities estimated by the model mentioned above would follow an expected order as $n_B > n_{BRL} > n_{ABR}$. Compared to ABR and BRL theories, the Bohm model considers a very thin planar sheath. Therefore, it underestimates the ion collecting area and overestimates the plasma density. Unlike the ARB model, the BRL model takes into account the orbital motion of the plasma ions. Consequently, n_{BRL} falls in between n_{ABR} and n_B. Although it is not shown explicitly in the results, the relation $n_B > n_{BRL} > n_{ABR}$ is checked for all measurements.

The usual criterion of minimizing the *fitting error* in the parametrization of the I-V characteristic curves has been applied for all theories. In general, a good agreement has been reached except at the far field of the plasma beam, far away from the thruster. There, the plasma density is smaller, and the Debye length could be already large in comparison to LP radius, and the use of the same single LP could be mistrusted.

The axial structures of the plasma density, plasma potential, and ion current density have been compared against the theoretical results of DiMagNo model [12]. This is a stationary two-fluid model (for electrons and ions) of a quasineutral and collisionless plasma. DiMagNo solves the supersonic expansion of the plasma throughout the divergent MN, by using the method of characteristics. It takes as input the normalized radial profiles of the plasma density, potential, electron temperature, and ion Mach number at the MN throat or at a certain section on the divergent side (ions must be slightly supersonic). These initial conditions are then propagated downstream, and intermediate points can be found by interpolation. Measured radial profiles of the plasma parameters at $z = 40$ mm have been used as the input (initial section) for DiMagNo. For

the Mach number, the value on-axis has been taken from axial measurements, being this about 2 and the direction is assumed to be parallel to the magnetic field lines. For the current case, it is a reasonable assumption because of its proximity to the MN throat.

This theoretical model also requires to choose a polytropic coefficient γ for describing the electrons thermodynamic, as it is usually done in the study of a hot gas expansion [18]. This is bounded between $\gamma = 1$, being the isothermal approach, and $\gamma = 5/3$, which is the adiabatic limit. For the current comparison $\gamma = 1.1$ is taken, because it yields the best fitting between the experimental and the theoretical results.

Some simulated plasma properties are compared against the corresponding experimental results in Figures 4 and 5. Density measurements acquired with the LP deviate from the theoretical results, and density seems to be overestimated far downstream. Due to the supersonic nature of the flow, and the fact that the LP is aligned with it, the disagreement might be supported by collisional processes, such as the charge-exchange collisions. To correct this, a combined FP-EP measure is performed, and density is estimated as $n = j_{iz}/u_{iz}e$. j_{iz} is the axial ion current density on-axis, which is directly measured by the FP; e is the electron-ion charge; and u_{iz} is the ion velocity, which is estimated by assuming that the ion energy is preserved throughout the expansion and the ion flow is sonic at the magnetic throat. These hypotheses combined with the direct measurements of the plasma potential ϕ using the EP allows determining u_{iz} as well as the Mach number, $M_{iz} = u_{iz}/c_s = \sqrt{1 + e(\phi_0 - \phi)/kT_e}$, being $c_s = \sqrt{kT_e/m_i}$ the ion sound speed, m_i is the ion particle mass, and k is the Boltzmann constant. Using this second approach, the axial density profile shows a good agreement with DiMagNo numerical results.

The mentioned direct measurements of the ion current density j_i and plasma potential ϕ are depicted in Figure 5, showing a good agreement with the theoretical model. Consequently, this justifies the use of the second approach for the estimation of the plasma density, as well as it unveils the need of exploring second order effects on the LP theories when this kind of probe is immersed

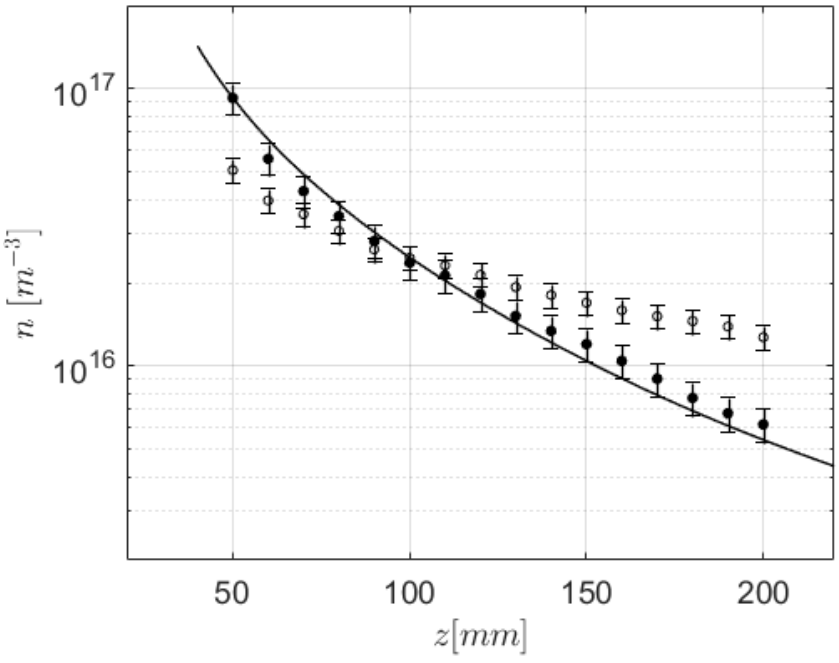

Figure 4: Axial profiles of the plasma density. The solid line corresponds to the DiMagNo model results. Empty circles depict the trend of the plasma density based on the LP measurements. Filled circles is the density computed with a combination of FP and EP measurements, as explained in the main text. These profiles have been obtained with the following HPT05 configuration: $\dot{m} = 50$ sccm of Argon, $P_{RF} = 500$ W, and the magnetic field B is generated by feeding the solenoids S1/S2/S3 with -5.3/12/16 Amps respectively (hereafter, nominal configuration).

within a magnetized and supersonic plasma plume.

Plasma density n and electron temperature T_e have been measured at the HPT05 exit section for different Argon mass flow rates $\dot{m}$, and $P_{RF} = 800$ W, as depicted in Figure 6. Plasma density increases one order of magnitude, from below 10^{17} up to close to 10^{18} m^{-3}, within the 40-60 sccm range. At larger mass flow rates, the plasma density increases slightly with $\dot{m}$. The measured electron temperature is $T_e = 4$ eV approximately, and remains almost constant with the increase of $\dot{m}$ above 60 sccm. The higher T_e for smaller $\dot{m}$ could be induced by

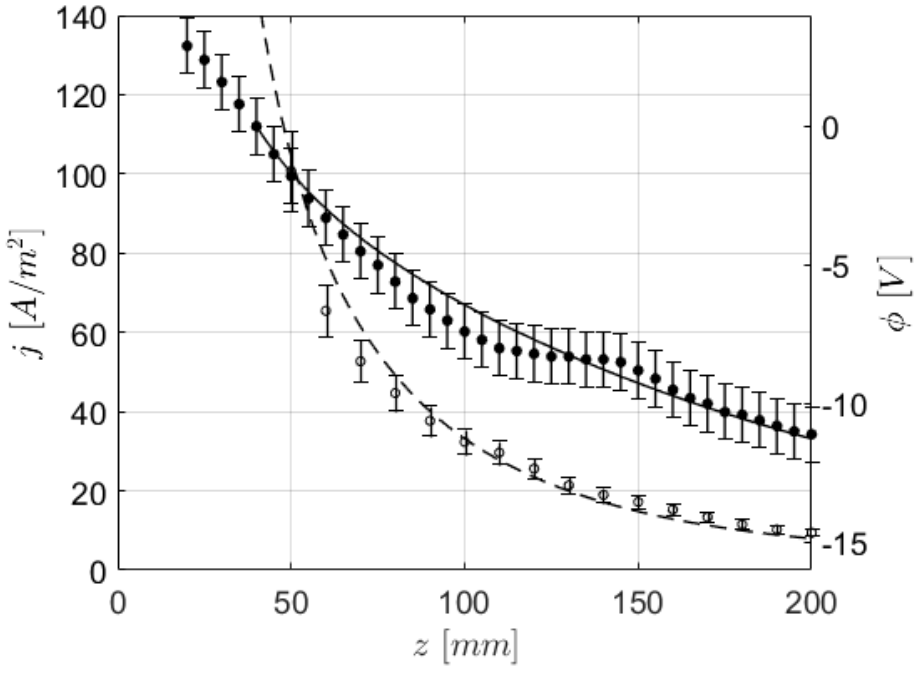

Figure 5: Axial profiles of the plasma potential, $\phi(z)$ (filled circles), and the axial ion current density, $j_{iz}(z)$ (open circles). Solid and dashed lines are for the DiMagNo theoretical results, $\phi(z)$ and $j_{iz}(z)$ respectively. These results are obtained for the same experimental conditions detailed in Figure 4.

the fact that the fitting error in the parametrized I-V curves presents a larger error when the plasma density is low.

Ion current density profiles, j_{iz}, have been obtained by sweeping the FP along the transverse direction, x, at $z = 200$ mm. Because the probe is moving along x, it is necessary to correct the collected current. This correction depends on $cos^3\theta$, with $\theta = tan^{-1}(x/z)$. Taking this adjustment, the radial current is $j_{ir}(\theta) = j_{iz}/cos^3\theta$. This radial current is referred to a polar frame $(r-\theta)$ centred at the HPT05 exit section centre. In Figure 7, some ion current profiles $j_{ir}(\theta, P_{RF})$ are depicted for different power levels. Each profile is normalized with the maximum measured current, $j_{ir,max} = \max(j_{ir}(\theta, P_{RF}))$, at the corresponding power level. Surprisingly, the normalized profiles do not depend on power. This means that

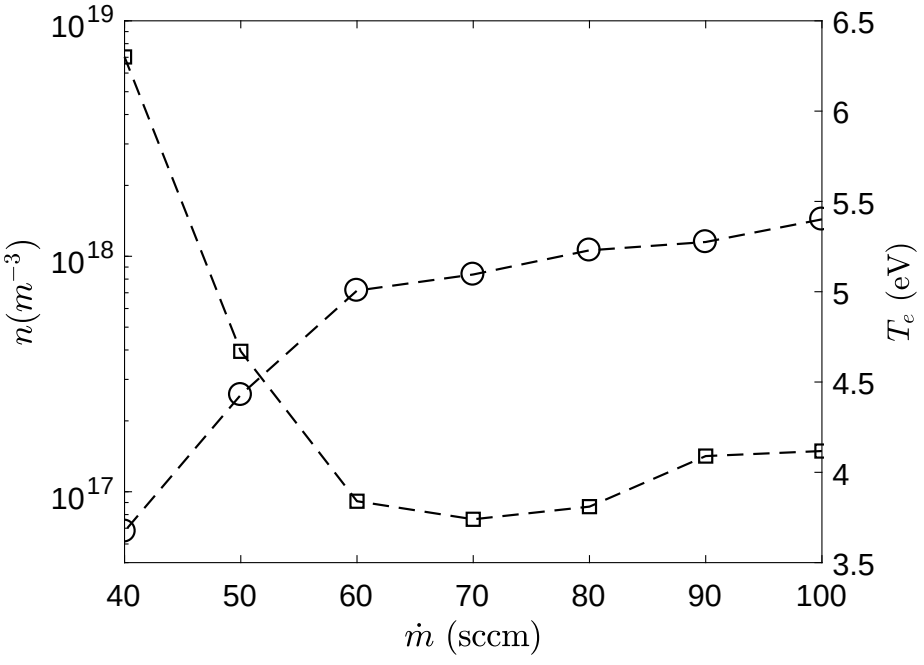

Figure 6: Plasma density (circles, left axis) and electron temperature (squares, right axis) measured at the exit section of the HPT05, $z = 0$ mm, as a function of the Argon mass flow rate. RF power is kept constant, $P_{RF} = 800$ W. The magnetic field is the nominal one (see Figure 4 caption). The chamber pressure increases almost linearly from $2.5 \cdot 10^{-5}$ mbar (40 sccm) to $5 \cdot 10^{-5}$ mbar (100 sccm).

no power is deposited onto the plasma in the MN area, instead, all the power is coupled within the discharge chamber. Also note that these profiles are double peaked, which is the common shape for RF inductive plasmas [19]. The effect of the outer coil (shaping the MN) on the beam collimation is illustrated as well. Beam divergence clearly increases when the magnetic nozzle is turned off as shown in Figure 7; this is even noticeable by visual inspection.

The total ion current carried by the plasma, I_i, can be estimated as the integral of the ion current density profiles $j_i(\theta)$ through the surface S, $I_i = \int_S \mathbf{j} \cdot \mathbf{dS}$. Note that S should be a semi-sphere centred at the HTP05 exit section in order to cover the whole plasma beam. However, in our case, this

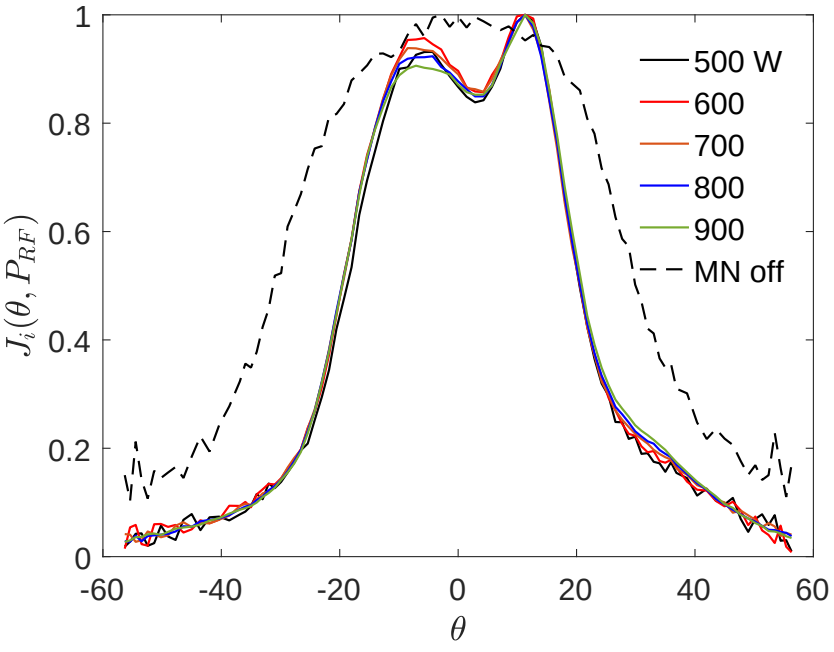

Figure 7: Normalized ion current density profile $J_i(\theta, P_{RF}) = j_{ir}/j_{ir,max}$ measured at $z =$ 200 mm, $\dot{m} = 50$ sccm of Argon, and the nominal magnetic field. The dashed line corresponds to the case for which the MN solenoid (S3) is turned off (other solenoids currents are the same as in the nominal configuration) and the power is $P_{RF} = 500$ W.

is limited by the capabilities of the probe arm system. Furthermore, in our computations we assume that the plasma beam is axisymmetric. If the beam is only composed of singly charged ions, then I_i is proportional to the mass flow rate of ions, $\dot{m}_i = m_i I_i/e$. The propellant utilization efficiency, $\eta_u = \dot{m}_i/\dot{m}$, measures the effectiveness of the HPT05 on ionizing the Argon neutral gas. This must be high for an electrodeless thruster to be competitive. In Figure 8, the dependence of η_u with the increase of P_{RF} is depicted. In this analysis, the Argon mass flow rate is kept constant at 50 sccm, and the magnetic topology is generated by applying $-5.3/12/16$ Amp of direct-current to the electromagnets S1/S2/S3 respectively. $\eta_u(P_{RF})$ monotonically rises with no bounds. Moreover, $\partial\eta_u/\partial P_{RF}$ diminishes with P_{RF}, pointing out the need to trade-off the optimum

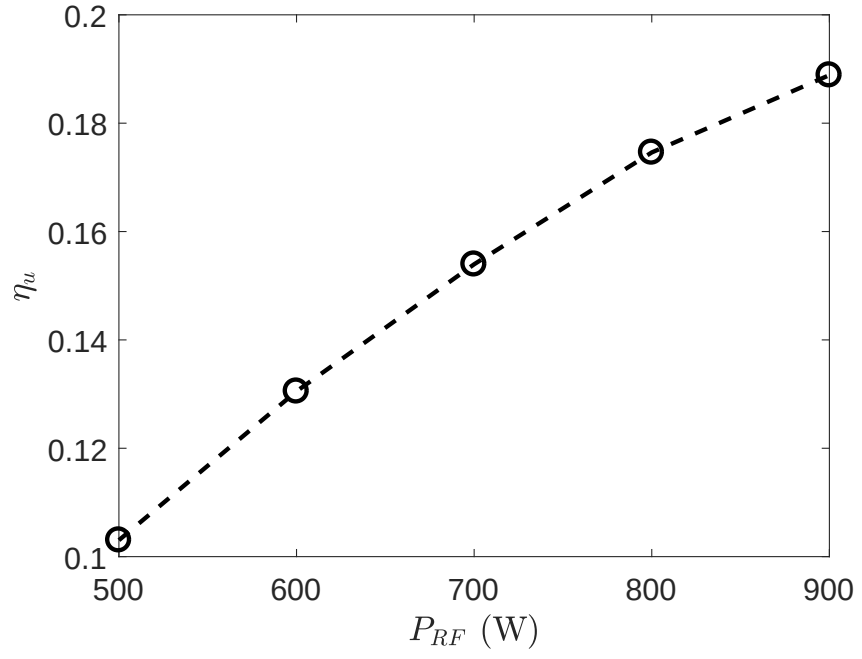

Figure 8: Utilization efficiency $\eta_u(P_{RF})$ as a function of the delivered RF power. The Argon mass flow rate is constant at $\dot{m}_{Ar} = 50$ sccm and the magnetic field is the nominal one.

power P_{RF} for given $\dot{m}$ and magnetic topology.

To conclude with the results, the HPT05 thrust, F, has been indirectly estimated as:

$$F = \int_s M_{zz} dS, \tag{1}$$

being $M_{zz} = m_i n u_{iz}^2 + nT_e$ the axial plasma momentum, which is integrated in an axisymmetric surface as it has been done in the integration of j_i to get I_i. F is evaluated at $z = 200$ mm, resulting $F = 6.6$ mN, for 500 W and $\dot{m} = 50$ sccm of Argon (equivalent to 1.5 mg/s). Consequently, the HPT05 thrust efficiency is $\eta_t = F^2/2\dot{m}P_{RF} = 2.9$ %, which is quite poor in comparison to other electric propulsion thrusters [20]. Potential sources of thrust inefficiency likely rely on a combination of several issues. First, the ionization degree is low as indicated by η_u, meaning that the current HPT05 design is either not well sized or the RF power is not well coupled to the plasma. Second, for the tested magnetic

topology it is known that plasma is not well screened from the walls, leading possibly to large plasma wall losses and recombination. Third, it has been noticed that the RF subsystem does not deliver the full power due to resistive losses induced by the thermal heating of the antenna and other components. In order to improve the thruster performances, apart from solving the mentioned issues, it would be interesting to understand better the wave-plasma coupling mechanism. Besides, theoretical models of the Helicon mode propagation in a complex magnetic topology, such the one in the HPT05 breadboard, have not been identified in the literature. Finally, as a promising result, we point out the good correlation between some of the measured plasma properties and the MN theoretical models.

Acknowledgements

Authors thanks Airbus Defence and Space for funding the experimental campaign (Contract No. CW241842), and SENER Ingeniería y Sistemas for its support to the prototype development and testing. Additional funds come from the Government of Spain, National Development and Research Program, Grant No. ESP2016-75887.

References

[1] C. Charles, R. Boswell, Current-free double-layer formation in a high-density helicon discharge, Applied Physics Letters 82 (2003) 1356–1358.

[2] O. Batishchev, Minihelicon plasma thruster, IEEE Transaction on Plasma Science 37 (2009) 1563–1571.

[3] D. P. et al, Thruster development set-up for the Helicon Plasma Hydrazine COmbined Micro research project (HPH.COM), 32nd International Electric Propulsion Conference, Wiesbaden, Germany, paper IEPC-2011-241, (2011).

[4] R. Boswell, Very efficient plasma generation by whistler waves near the lower hybrid frequency, Plasma Physics and Controlled Fusion 26 (1984) 1147–1162.

[5] F. Chen, Plasma ionization by helicon waves, Plasma Physics and Controlled Fusion 33 (1991) 339.

[6] D. Goebel, I. Katz, Fundamentals of electric propulsion: ion and Hall thrusters, Wiley, (2008).

[7] C. Charles, R. Boswell, M. Lieberman, Xenon ion beam characterization in a helicon double layer thruster, Applied Physics Letters 89 (2006) 261503.

[8] K. Takahashi, T. Lafleur, C. Charles, P. Alexander, R. Boswell, Electron diamagnetic effect on axial force in an expanding plasma: Experiments and theory, Physical Review Letters 107 (2011) 235001.

[9] J. M. Little, E. Y. Choueiri, Critical condition for plasma confinement in the source of a magnetic nozzle flow, IEEE Transactions on Plasma Science 43 (2015) 277–286.

[10] M. Merino, E. Ahedo, Contactless steering of a plasma jet with a 3d magnetic nozzle, Plasma Sources Sci. Technol 26 (2017) 095001.

[11] E. Ahedo, J. Navarro-Cavalle, Helicon thruster plasma modeling: Two-dimensional fluid-dynamics and propulsive performances, Physics of Plasmas 20 (2013) 043512.

[12] E. Ahedo, M. Merino, Two-dimensional supersonic plasma acceleration in a magnetic nozzle, Physics of Plasmas 17 (2010) 073501.

[13] B. Tian, E. Ahedo, J. Navarro-Cavalle, Investigation of plasma-wave interaction in helicon antenna thrusters, 50th Joint Propulsion Conference & Exhibit, AIAA Paper, 2014-3475, (2014).

[14] M. M. Navarro-Cavalle, E. Ahedo, M. Ruiz, V. Sánchez, Design of helicon plasma thruster subsystems, 50th Joint Propulsion Conference & Exhibit, AIAA Paper, no. 2014-3699, (2014).

[15] J. G. Laframboise, Theory of spherical and cylindrical Langmuir probes in a collisionless, Maxwellian plasma at rest, Tech. rep., of the Toronto University (Ontario), Institute for Aerospace Studies (1966).

[16] J. Allen, R. Boyd, P. Reynolds, The collection of positive ions by a probe immersed in a plasma, Proceedings of the Physical Society. Section B 70 (3) (1957) 297.

[17] D. Bohm, The characteristics of electrical discharges in magnetic fields, MacGraw-Hill, New York, (1949), p. 77.

[18] G. Sutton, O. Biblarz, Rocket propulsion elements, Wiley, (2010).

[19] M. Lieberman, A. Lichtenberg, Principles of plasma discharges and materials processing, Wiley-Blackwell, (2005).

[20] M. Martínez-Sánchez, J. Pollard, Spacecraft electric propulsion–an overwiew, J. Propulsion and Power 14 (1998) 688–699.